The Role of Carrier Injection in the Breakdown Mechanism of Amorphous Al_2O_3 Layers

P. La Torraca, A. Padovani, *Member*, *IEEE*, J. Strand, A. Shluger, L. Larcher

***Abstract*—We investigated the dielectric breakdown (BD) mechanism in amorphous alumina (a-Al_2O_3) metal-insulator-metal (MIM) stacks. Density functional theory (DFT) calculations reveal that oxygen vacancy (V_O) generation in a-Al_2O_3 occurs via thermochemical (TC) bond-breaking and, more efficiently, via newly discovered pathways enabled by charge trapping in under-coordinated Al ions (UC_{Al}s) and in existing V_Os. Multiscale simulations show the importance of these processes, which allow explaining the experimental BD dynamics in a-Al_2O_3, and provide valuable insights into the role of carriers' injection in the degradation and reliability of high-k materials.**

***Index Terms*— Amorphous alumina, atomic defects, breakdown, carrier injection, high-k dielectric**

I. Introduction

DESPITE the widespread applications of a-Al_2O_3 as a high-k gate oxide [1-3], and in signal [4] and memory capacitors [5,6], its degradation mechanism is still unclear. The current understanding is based on the TC model of bond-breaking [7,8], according to which current-carrying defects, such as V_Os, are generated by the rupture of the Al-O bonds as a result of an electric field application and the dielectric's polarization. A bond-breaking activation energy (E_A) around 2.4 eV was extracted from experimental results on a-Al_2O_3 [8]. In contrast, for a stable pair of V_O and O interstitial (O_i) in crystalline α-Al_2O_3, formation energies between 5.8 and 11.8 eV have been calculated [9-11], with the corresponding bond-breaking E_As even higher. Although different E_As are expected for the different Al_2O_3 phases, the huge discrepancy (>3 eV) suggests the involvement of other processes in BD. For example, according to the carrier injection (CI) breakdown model [12], the injection and localization of carriers in perfect or defective lattice can weaken the adjacent metal-oxygen bonds, promoting field-induced bond-breaking processes and enabling generation on new V_Os. The effectiveness of the CI mechanism has been shown in SiO_2 [12] and HfO_2 [13].

In this work, we show that the CI mechanism can correctly describe dielectric BD in a-Al_2O_3 MIM stacks while reconciling the theoretical and experimental E_As. DFT calculations are used to characterize a-Al_2O_3 defects and their generation processes,

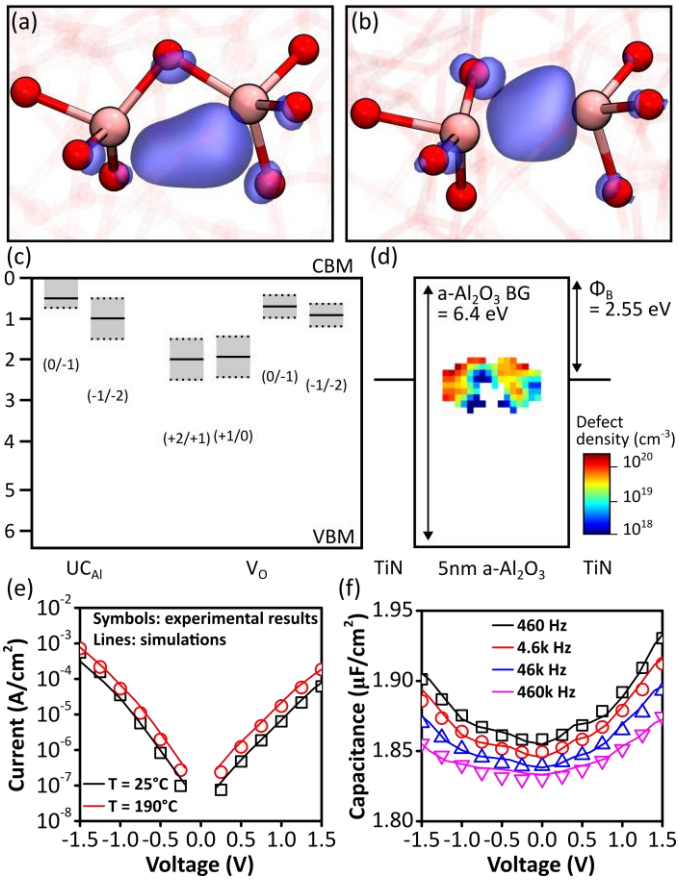

Figure 1. (a) Structural and electronic configuration of an UC_{Al} and (b) of an V_O in a-Al_2O_3. Pink and red atoms are Al and O, respectively. An iso-surface of the electron wavefunction is shown in blue. (c) The calculated charge transition levels (corresponding to thermal ionization energies E_{TH}s) ranges for V_Os and UC_{Al}s in a-Al_2O_3, with solid black lines showing the distributions' median values; (d) extracted space-energy defect distribution in a 5 nm TaN/a-Al_2O_3/TaN MIM stack, compatible with +2/+1 and +1/0 transition of V_Os; (e) current and (f) capacitance simulation of the 5 nm TaN/a-Al_2O_3/TaN MIM stack.

showing how the injection on electrons into structural precursor sites, formed by UC_{Al}s or existing V_Os, greatly facilitate the creation of new V_Os. Using the commercial simulation software Ginestra® [14], we show that the resulting electrical characteristics and BD statistics agree with the experimental results, strongly supporting the importance of electron injection for the a-Al_2O_3-based devices' reliability.

P. L.T. is with the Department of Science and Methods for Engineering, University of Modena and Reggio Emilia, Reggio Emilia, Italy and with the Tyndall National Institute, University College Cork, Cork, Ireland. (e-mail: paolo.latorraca@tyndall.ie)

A. P. is with the Engineering Department "Enzo Ferrari", University of Modena and Reggio Emilia, Reggio Emilia, Italy.

J. S. and A. S. are with the Department of Physics and Astronomy, University College London, London, United Kingdom.

L. L. is with Applied Materials – MDLx Italy R&D, Reggio Emilia, Italy.

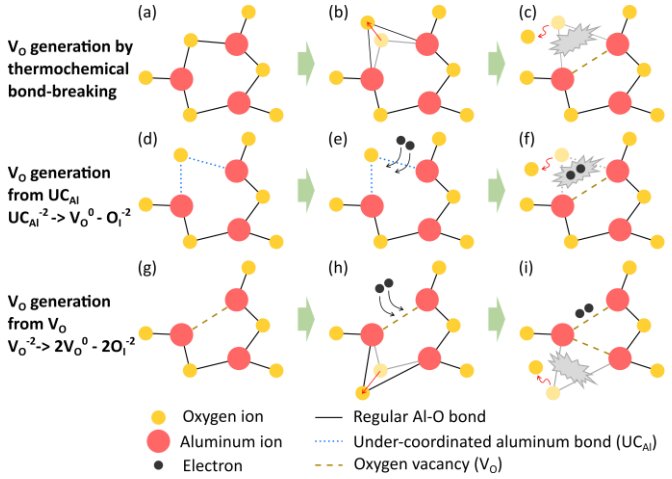

Figure 2. Schematic representation of different V_Os generation pathways: a typical O-Al-O bond (a) stretched by an electric field (b) breaks generating a V_O (c); a structural precursor site (d) traps two electrons (e) facilitating the creation of V_O - O_I^{2-} pair (f); a V_O (g) traps two electrons (h), facilitating the creation of the second V_O and O_I^{2-} ion (i). The TC model only accounts for the former process (a-c), while the CI model includes all three depicted processes.

II. Density Functional Theory Calculations

DFT calculations are carried out using the CP2K software package [15]. The exchange-correlation (XC) energy is calculated using the PBE0-TC-LRC functional [16], providing a more accurate description of the electronic structure and the localized states of oxides compared to standard Generalized Gradient Approximation (GGA) functionals. We use the DZVP-MOLOPT-SR-GTH [17] basis set for both O and Al, with the Goedecker-Teter-Hutter pseudopotentials [18]. The a-Al_2O_3 structures are produced using the melt-and-quench method, as described in [19]. As described in [19], a non-local exchange fraction of 0.25 and a cutoff distance of 3 Å provide a functional that complies with the Koopmans' theorem. This XC functional results in band gaps (BG) in the 6 to 7 eV range. The analysis of the electronic properties of a-Al_2O_3 models showed that V_Os and pairs of 4-coordinated Al ions (i.e. UC_{Al}s) can trap electrons in states within the a-Al_2O_3 BG. Examples of the electronic and structural configurations forming at UC_{Al}s and V_Os are shown in Fig.1(a) and (b), respectively. Due to disorder of amorphous structures, the respective thermal ionization energies (E_{TH}s) and relaxation energies (E_{REL}s) form distributions, which is estimated by sampling different sites for the respective defects across 10 different a-Al_2O_3 models. The values for these energies are reported in Table I, and the E_{TH}s positions within the a-Al_2O_3 BG are shown in Fig.1(c).

TABLE I
A-AL2O3 DEFECTS' AND DEGRADATION PROCESSES' PARAMETERS

Parameter	DFT results	VDDB simulations
UC_{Al}		
-1/-2 E_{TH} / E_{REL}	0.5–1.6 eV / 0.5–1.6 eV	0.9–1.9 eV / 1.0 eV
0/-1 E_{TH} / E_{REL}	0–0.7 eV / 0–0.7 eV	0.4–1.4 eV / 1.0 eV
V_O		
-1/-2 E_{TH} / E_{REL}	0.6–1.2 eV / 1.1–1.9 eV	0.8–1.8 eV / 1.5 eV
0/-1 E_{TH} / E_{REL}	0.4–1.0 eV / 0.9–1.7 eV	0.6–1.6 eV / 1.3 eV
+1/0 E_{TH} / E_{REL}	1.4–2.4 eV / 1.1–2.1 eV	1.3–3.3 eV / 1.6 eV
+2/+1 E_{TH} / E_{REL}	1.5–2.5 eV / 0.5–1.5 eV	1.4–3.4 eV / 1.0 eV
TC bond breaking E_A	3.0–6.0 eV	4.3 eV
UC_{Al}^{-2} -> $V_O^0 - O_I^{-2}$ E_A	2.0–3.0 eV	2.5 eV
V_O^{-2}-> $2V_O^0 - 2O_I^{-2}$ E_A	3.0 eV	2.8 eV

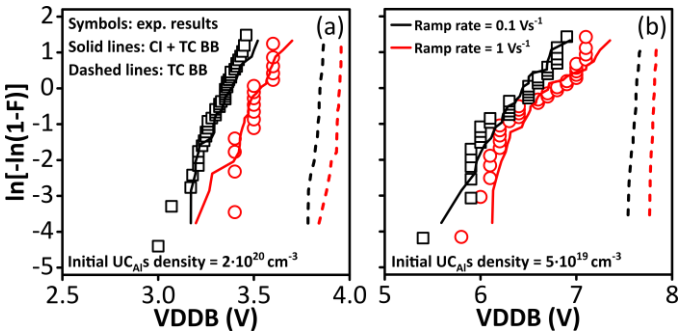

Figure 3. Experimental (symbols) and simulated (lines) VDDB distributions of (a) 5 nm and (b) 10 nm TaN/a-Al_2O_3/TaN stacks [8], under RSV with 0.1 Vs^{-1} (black) and 1 Vs^{-1} (red) ramp rate. Simulations are obtained with the bond-breaking EAs presented in this work (Table I). The TC bond-breaking process (TC model, in dashed lines) alone overestimates the VDDB. Including the bond-breaking processes enabled by charge trapping at the defects (CI + TC model, in solid lines), shown in Fig. 2, allow reproducing the VDDB statistics. The statistical spread is reproduced considering different UC_{Al}s initial densities.

The bond breaking process is simulated in different a-Al_2O_3 structures using the nudged elastic band (NEB) method [20], including the effect of the electric field [21]. The most relevant V_Os generation processes identified from the simulations are depicted in Fig. 2 and the respective E_As are summarized in Table I. In the simulated systems, the TC bond-breaking process creates $V_O^{+2} - O_I^{-2}$ pairs, Fig. 2(a-c). While not requiring electron localization, this process is characterized by a relatively high bond-breaking E_As range. The negative charging of UC_{Al}s and V_Os from CI into their shallow states enables more efficient V_Os generation pathways. Double electron trapping in a UC_{Al}s, Fig. 2(d-f), lowers the bond-breaking E_A facilitating the generation of V_Os through the conversion of UC_{Al}^{-2}s into $V_O^0 - O_I^{-2}$ pairs. Pre-existing V_Os, either present in the pristine system or generated by the electrical stress, are also identified as precursor sites for new V_Os. Quadruple electron trapping in a pre-existing V_O induces a distortion in the adjacent bonds, lowering their bond-breaking E_A and thus facilitating the generation of a new V_O, Fig 2(g-i). Although only a small share of V_Os (~ 1%) are stable in the negative charge states, required to enable the described process, all poly-vacancy clusters are capable of negative charging, facilitating the generation of V_Os, as shown in Fig. 2(g-i).

III. Multiscale Simulations

The results of DFT calculations were used to investigate the a-Al_2O_3 BD dynamics of TaN/a-Al_2O_3/TaN MIM with Ginestra® [14]. This approach allows us to self-consistently include the electrostatics of devices, the trapping and transport of carriers (according to the multiphonon trap-assisted tunneling model [22]), and the degradation processes illustrated in Fig. 2. Fig. 1(b) shows the space-energy defect distribution of a 5 nm TaN/a-Al_2O_3/TaN MIM stack, extracted via defect spectroscopy from the current-voltage (IV) curves, Fig. 1(c), and capacitance-voltage (CV) curves, Fig. 1(d), reported in [8]. The extracted defects' E_{TH} is distributed from 1.9 eV to 3.2 eV, peaking near 2.0 eV, which is consistent with the DFT results for the (+2/+1) and the (+1/0) transition levels of V_Os. As in SiO_2 [23,24] and HfO_2 [22,24], V_Os are thus recognized as the main defects involved in electron transport and trapping in a-

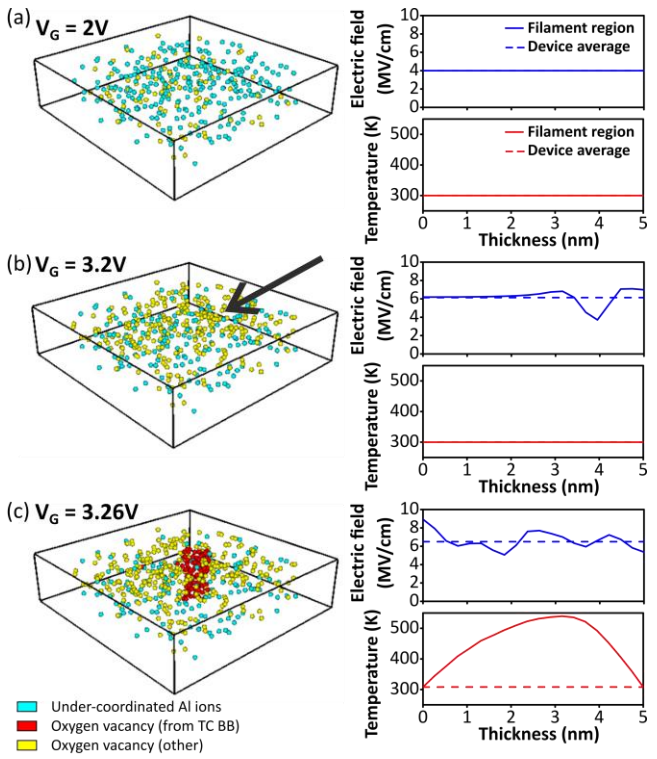

Figure 4. Breakdown dynamics in a 5nm TaN/a-Al_2O_3/TaN MIM. Starting from a pristine device with V_Os and UC_{Al}s distributions, the defect generation starts at approximately 4 $MVcm^{-1}$ (a) via CI-related processes alone. Upon the formation of a large V_Os cluster (b) the oxide local permittivity is reduced, enhancing the surrounding electric field and initiating the TC bond breaking. A conductive filament is rapidly formed (c), driving an increasingly higher current. The resulting increment of the local temperature facilitates the TC V_Os generation, initiating a thermal runway that ends in the device hard breakdown.

Al_2O_3. The shallower transition levels of V_Os and UC_{Al}s do not contribute to the transport nor to the AC response in the voltage range considered in Fig. 1. This highlights the elusive nature of the UC_{Al}s, which cannot be effectively detected and characterized with regular electrical characterization techniques (e.g. IV or CV measurements). Nevertheless, their effects could be observed in the oxide degradation dynamics: the application of a sufficiently high field allows charge trapping and transport even in such shallow levels, possibly triggering the CI-related degradation processes described in the Section II and Fig. 2.

The breakdown dynamics and the critical role played by UC_{Al}s and V_Os is investigated by simulating the voltage dependent dielectric breakdown (VDDB) statistics of 5 nm and 10 nm TaN/a-Al_2O_3/TaN MIM stacks under ramped voltage stress (RVS) at different ramp rates (0.1 and $1Vs^{-1}$), also reported in [8]. For the sake of simplicity, the simulations were performed considering uniform distributions of the E_{TH}s and single valued E_{REL}s and E_As, as reported in Table I. The E_{REL}s were selected as mean values of the distributions calculated in DFT, while the mean and spread of E_{TH}s distributions, and the E_As of defect generation processes, were optimized to fit the experimental results. The optimal E_{TH}s values are in reasonable agreement with the ranges obtained from DFT calculations. The small discrepancy seen in Table I can be ascribed to the adoption of a single valued E_{REL}s, or to small differences in the electrodes work functions. A large E_{TH} spread was considered in V_Os (+2/+1) and (+1/0) transitions for consistency with [8]. The E_As values are in good agreement with results of the DFT calculations. Fig. 3 shows the simulation results obtained considering the TC bond breaking process alone (dashed lines) and by including the CI-related degradation processes (solid lines), i.e. all processes depicted in Fig. 2. The sole TC bond breaking process greatly overestimates the BD voltages and cannot explain the lower Weibull slope in the 10 nm stack. Including the CI-related degradation processes, the whole VDDB statistics is correctly reproduced. The pathways enabled by the CI allow for a more efficient V_O generation, facilitating the BD process and thus reducing the BD voltage. The lower slope exhibited by the 10 nm stack results from a lower UC_{Al}s density in the pristine device: in a less defective device, a larger number of defects must be generated to form a BD spot, increasing the statistical variability of the degradation process, which translates in a lower Weibull slope [24]. This result agrees with previous results on a-Al_2O_3 based on the IV curve fitting [8], showing a higher defectivity in a 5 nm layer than in 10 nm and 20 nm layers. The origin of higher initial UC_{Al}s density in the thinner device cannot be clearly identified. It can be ascribed to the larger impact of the defect-rich interfaces on the overall defect distribution, having a stronger impact on thin layers [25], and possibly to the different growth time and thermal budget experienced by the a-Al_2O_3 layers.

Fig. 4 shows the degradation process in the 5 nm a-Al_2O_3 stack. In a pristine device, Fig. 4(a), both V_Os and UC_{Al}s are present, with the former contributing to the leakage current shown in Fig. 1(c). At approximately 4$MVcm^{-1}$ (2 V), the CI into the UC_{Al}s enables the generation of new V_Os, which in turn can also generate new V_Os, following the pathways shown in Fig. 2. The relatively low E_As of these mechanisms provide an efficient and self-sustaining generation of V_Os, without the TC bond-breaking contribution. This generation process leads to the formation of V_Os clusters close to the location of the starting UC_{Al}s. When a sufficiently large cluster of V_Os is formed, Fig. 4(b), the permittivity reduction associated to the metallic nature of that cluster leads to the redistribution of the internal electric field. A significant enhancement of the electric field above and below the V_Os cluster is sufficient to trigger the TC bond breaking in these regions, longitudinally extending the cluster into a full BD spot, Fig.4(c). The current flowing in the BD spot increases the local temperature, further facilitating the V_O generation, with thermal runway resulting in the hard BD.

IV. Conclusions

Our comprehensive study, including DFT calculations and multiscale simulations, consistently explains the carrier transport and the breakdown dynamics in a-Al_2O_3 MIM stacks within the CI model framework. The transport in the considered a-Al_2O_3 MIM stacks is dominated by trap-assisted tunneling through deep V_Os states. The efficient generation of V_Os is enabled by electron injection into pre-existing UC_{Al}s and V_Os. This model reproduces the VDDB statistics of a-Al_2O_3 MIM stacks, and provides an explanation for the discrepancy between the theoretical TC bond-breaking E_A values and the experimental results.

REFERENCES

[1] T. L. Newsom, C. R. Allemang, T. H. Cho, N. P. Dasgupta and R. L. Peterson, "59.9 mV·dec Subthreshold Swing Achieved in Zinc Tin Oxide TFTs With In Situ Atomic Layer Deposited AlO Gate Insulator," in IEEE Electron Device Letters, vol. 44, no. 1, pp. 72-75, Jan. 2023, doi: 10.1109/LED.2022.3219351.

[2] Y. -C. Chien et al., "Origin of High Current and Illumination Stress Instability in Self-Aligned a-InGaZnO Thin Film Transistors With Al2O3 as High-κ Gate Dielectric," in IEEE Electron Device Letters, vol. 41, no. 4, pp. 565-568, April 2020, doi: 10.1109/LED.2020.2976616.

[3] M. -J. Yu, R. -P. Lin, Y. -H. Chang and T. -H. Hou, "High-Voltage Amorphous InGaZnO TFT With Al2O3 High-k Dielectric for Low-Temperature Monolithic 3-D Integration," in IEEE Transactions on Electron Devices, vol. 63, no. 10, pp. 3944-3949, Oct. 2016, doi: 10.1109/TED.2016.2598396.

[4] S.Y. Ko, J.I. Oh, J.C. Choi, K.H. Lee, Y.H. Bae, Y.C. Jung, Y.H. Lee, MIM Capacitors Using ALD Al 2 O 3 for RF IC and DRAM Applications, MRS Proc. 833 (2004) 2–6, doi: 10.1557/proc-833-g3.10.

[5] S.Y. Lee, J. Chang, J. Choi, Y. Kim, H.J. Lim, H. Jeon, H. Seo, Investigation of ultrathin Pt/ZrO2–Al2O3–ZrO2/TiN DRAM capacitors Schottky barrier height by internal photoemission spectroscopy, Curr. Appl. Phys. 17 (2017) 267–271, doi: 10.1016/j.cap.2016.12.004.

[6] J. Park, S. Heo, J. Chung, G.-S. Park, Electron Energy Loss Spectroscopy Characterization of TANOS (TaN/Al2O3/Si3N4/SiO2/Si) Stacks, Microsc. Microanal. 19 (2013) 109–113, doi: 10.1017/S1431927613012440.

[7] J. W. McPherson, Jinyoung Kim, A. Shanware, H. Mogul and J. Rodriguez, "Trends in the ultimate breakdown strength of high dielectric-constant materials," in IEEE Transactions on Electron Devices, vol. 50, no. 8, pp. 1771-1778, Aug. 2003, doi: 10.1109/TED.2003.815141.

[8] P. La Torraca, F. Caruso, A. Padovani, G. Tallarida, S. Spiga and L. Larcher, "Atomic Defects Profiling and Reliability of Amorphous Al2O3 Metal–Insulator–Metal Stacks," in IEEE Transactions on Electron Devices, vol. 69, no. 7, pp. 3884-3891, July 2022, doi: 10.1109/TED.2022.3172928.

[9] X. Xiang, G. Zhang, X. Wang, T. Tang, and Y. Shi, "A new perspective on the process of intrinsic point defects in α-Al2O3," Physical Chemistry Chemical Physics, vol. 17, no. 43. Royal Society of Chemistry (RSC), pp. 29134–29141, 2015. doi: 10.1039/c5cp04867b.

[10] A. Kononov, C.-W. Lee, E. P. Shapera, and A. Schleife, "Identifying native point defect configurations in α-alumina," Journal of Physics: Condensed Matter, vol. 35, no. 33. IOP Publishing, p. 334002, May 18, 2023. doi: 10.1088/1361-648x/acd3cf.

[11] Y. F. Zhukovskii, A. Platonenko, S. Piskunov, and E. A. Kotomin, "Ab initio simulations on migration paths of interstitial oxygen in corundum," Nuclear Instruments and Methods in Physics Research Section B: Beam Interactions with Materials and Atoms, vol. 374. Elsevier BV, pp. 29–34, May 2016. doi: 10.1016/j.nimb.2015.08.087.

[12] A. Padovani, P. La Torraca, J. Strand, A. Shluger, V. Milo and L. Larcher, "Towards a Universal Model of Dielectric Breakdown," *2023 IEEE International Reliability Physics Symposium (IRPS)*, Monterey, CA, USA, 2023, pp. 1-8, doi: 10.1109/IRPS48203.2023.10117846.

[13] J. Strand, P. La Torraca, A. Padovani, L. Larcher, and A. L. Shluger, "Dielectric breakdown in HfO2 dielectrics: Using multiscale modeling to identify the critical physical processes involved in oxide degradation," Journal of Applied Physics, vol. 131, no. 23. AIP Publishing, p. 234501, Jun. 21, 2022. doi: 10.1063/5.0083189.

[14] Applied Materials Ginestra®. https://www.appliedmaterials.com/eu/en/semiconductor/solutions-and-software/software-solutions/ginestra-simulation-platform.html

[15] J. VandeVondele, M. Krack, F. Mohamed, M. Parrinello, T. Chassaing, and J. Hutter, "Quickstep: Fast and accurate density functional calculations using a mixed Gaussian and plane waves approach," Computer Physics Communications, vol. 167, no. 2. Elsevier BV, pp. 103–128, Apr. 2005. doi: 10.1016/j.cpc.2004.12.014.

[16] M. Guidon, J. Hutter, and J. VandeVondele, "Robust Periodic Hartree−Fock Exchange for Large-Scale Simulations Using Gaussian Basis Sets," Journal of Chemical Theory and Computation, vol. 5, no. 11. American Chemical Society (ACS), pp. 3010–3021, Oct. 20, 2009. doi: 10.1021/ct900494g.

[17] J. VandeVondele and J. Hutter, "Gaussian basis sets for accurate calculations on molecular systems in gas and condensed phases," The Journal of Chemical Physics, vol. 127, no. 11. AIP Publishing, Sep. 18, 2007. doi: 10.1063/1.2770708.

[18] S. Goedecker, M. Teter, and J. Hutter, "Separable dual-space Gaussian pseudopotentials," Physical Review B, vol. 54, no. 3. American Physical Society (APS), pp. 1703–1710, Jul. 15, 1996. doi: 10.1103/physrevb.54.1703.

[19] O. A. Dicks and A. L. Shluger, "Theoretical modeling of charge trapping in crystalline and amorphous Al2O3," Journal of Physics: Condensed Matter, vol. 29, no. 31. IOP Publishing, p. 314005, Jul. 06, 2017. doi: 10.1088/1361-648x/aa7767.

[20] H. Jónsson, G. Mills, and K. W. Jacobsen, "Nudged elastic band method for finding minimum energy paths of transitions," Classical and Quantum Dynamics in Condensed Phase Simulations. WORLD SCIENTIFIC, Jun. 1998. doi: 10.1142/9789812839664_0016.

[21] J. W. Strand, J. Cottom, L. Larcher, and A. L. Shluger, "Effect of electric field on defect generation and migration in HfO2," Physical Review B, vol. 102, no. 1. American Physical Society (APS), Jul. 21, 2020. doi: 10.1103/physrevb.102.014106.

[22] L. Vandelli, A. Padovani, L. Larcher, R. G. Southwick, W. B. Knowlton and G. Bersuker, "A Physical Model of the Temperature Dependence of the Current Through SiO2/HfO2 Stacks," in IEEE Transactions on Electron Devices, vol. 58, no. 9, pp. 2878-2887, Sept. 2011, doi: 10.1109/TED.2011.2158825.

[23] A. Padovani, D. Z. Gao, A. L. Shluger, and L. Larcher, "A microscopic mechanism of dielectric breakdown in SiO2 films: An insight from multi-scale modeling," Journal of Applied Physics, vol. 121, no. 15. AIP Publishing, p. 155101, Apr. 21, 2017. doi: 10.1063/1.4979915.

[24] A. Padovani and L. Larcher, "Time-dependent dielectric breakdown statistics in SiO2 and HfO2 dielectrics: Insights from a multi-scale modeling approach," 2018 IEEE International Reliability Physics Symposium (IRPS), Burlingame, CA, USA, 2018, pp. 3A.2-1-3A.2-7, doi: 10.1109/IRPS.2018.8353552.

[25] D. M. Fleetwood, "'Border traps' in MOS devices," in IEEE Transactions on Nuclear Science, vol. 39, no. 2, pp. 269-271, April 1992, doi: 10.1109/23.277495.